Inorganic Chemistry

pubs.acs.org/IC

Article

# Modular Imine Chelates with Variable Anionic Donors Promote Red Phosphorescence in Cyclometalated Iridium Complexes

Chenggang Jiang, Sungwon Yoon, Yennie H. Nguyen, and Thomas S. Teets*

Cite This: *Inorg. Chem.* 2023, 62, 11278−11286

Read Online

ACCESS | Metrics & More | Article Recommendations | Supporting Information



**ABSTRACT:** The lack of red and deep-red emitting molecular phosphors with high photoluminescence quantum yields remains a significant fundamental challenge and has implications in optoelectronic technologies for color displays and other consumer products. In this work, we introduce a series of seven new red or deep-red emitting heteroleptic bis-cyclometalated iridium(III) complexes, supported by five different ancillary ligands (L^X) from the salicylaldimine and 2-picolinamide families. Previous work had shown that electron-rich anionic chelating "L^X" ligands can be effective in supporting efficient red phosphorescence, and the complementary approach described here, in addition to being synthetically simpler, offers two key advantages over the previous designs. First, the "L" and "X" functionalities can be independently tuned, providing excellent control over the electronic energy levels and excited-state dynamics. Second, these classes of L^X ligands can have beneficial impacts on the excited-state dynamics but do not significantly perturb the emission color profile. Cyclic voltammetry experiments show that the substituents on the L^X ligand impact the HOMO energy but have a minimal effect on the LUMO energy. Photoluminescence measurements reveal that all the compounds luminesce in the red or deep-red region as a function of the cyclometalating ligand and exhibit exceptionally high photoluminescence quantum yields ($\Phi_{PL}$), comparable or superior to the best-performing red-emitting iridium complexes.

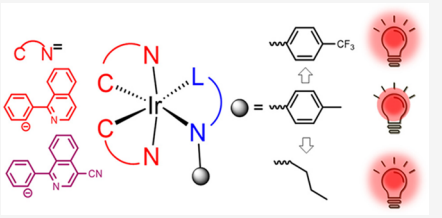


## INTRODUCTION

Since their discovery, cyclometalated iridium complexes have been extensively studied in various applications, such as biological probes,[1,2] photosensitizers,[3,4] catalysts,[5,6] and sensors.[7,8] The use of Ir(III) complexes as emitters in organic light-emitting diodes (OLEDs) is their most widely developed application.[9−12] Due to the strong spin−orbit coupling (SOC) induced by the heavy metal, iridium(III) complexes have relatively short excited state lifetimes among phosphorescent compounds and therefore are suitable for OLED applications.[13,14] Phosphorescent iridium complexes can often have near-unity quantum yields[15−18] in the green and yellow regions, and thus OLED devices with colors in these regions are very efficient and represent a low research priority in the display industry.

However, iridium complexes that emit in the red region typically have lower quantum yields, and those that have been doped into some of the most efficient red OLEDs have photoluminescence quantum yields near 0.5 in solution.[10,19,20] There are also other metal complexes have been explored in red to near-infrared phosphorescence, with high photoluminescence efficiency that makes them suitable for OLEDs.[21−23] These lower efficiencies in the red region stem from the energy gap law,[24] which dictates faster nonradiative decay rates ($k_{nr}$) in red emitters, as well as the cubic dependence of the radiative rate ($k_r$) on the transition energy, which results in a smaller $k_r$.[25] Therefore, augmenting phosphorescence quantum yields in the lower energy ranges of the visible spectrum is still a fundamental challenge, and improvements and new insights could lead to more efficient red OLEDs while benefiting the design of near-infrared phosphors that are critical for applications including night vision,[26] medical imaging,[27] and biological probes.[28]

One of the most well-studied classes of luminescent iridium complexes is the heteroleptic [Ir(C^N)$_2$(L^X)] structure, where C^N is the cyclometalating ligand and L^X is a monoanionic chelating ancillary ligand. Color tuning the phosphorescence is most often accomplished by the structure of the cyclometalating ligand,[29] but it has been recognized for some time that the ancillary L^X ligand can subtly influence the emission wavelength while having a large influence on redox properties and excited-state dynamics.[30] Our group has shown the impact that ancillary ligands can have in maximizing photoluminescence quantum yields in the red region and beyond,[31−34] and a few other groups have followed with related approaches.[35,36] Our strategy has centered on electron-rich, $\pi$-donating ancillary ligands, which destabilize the HOMO orbital, increase the metal d-orbital participation and SOC in the excited state, and augment $k_r$ values.[31,37] L^X ligands from the $\beta$-ketoiminate and amidinate families are

**Received:** May 30, 2023
**Published:** July 6, 2023

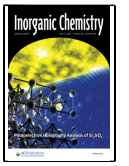






https://doi.org/10.1021/acs.inorgchem.3c01770
*Inorg. Chem.* 2023, 62, 11278−11286

particularly effective in this regard, but there are some key disadvantages. First, syntheses of these previous generations typically involve highly basic and moisture-sensitive alkali metal salts of the L^X ligands, and the electron-rich $Ir(C^N)_2(L^X)$ products are not amenable to chromatographic purification and at times not stable under ambient conditions. Second, the L^X ligands in most of our previous efforts were conjugated, making it impossible to independently tune the "L" and "X" functionalities. While in the end this may not be a detriment, the ability to separately perturb the "L" and "X" modalities was a fundamental interest of ours, and here, we show that it can be advantageous when optimizing red phosphorescence. Finally, the previous electron-rich L^X ligands we employed all engendered substantial red shifts in phosphorescence, so it was not possible to optimize excited-state dynamics without eroding the color profile.

Salicylaldimines and 2-picolinamides represent alternative classes of L^X ligands that have been used in a few reports to support luminescent cyclometalated iridium complexes. Salicylaldimine complexes can exhibit enhanced red phosphorescence in the solid state[38−40] and circularly polarized luminescence,[41] whereas 2-picolinamide analogues phosphoresce in the green to yellow regions.[42−45] One common feature of these recent reports is the use of 2-phenylpyridine or fluorinated 2-phenylpyridine C^N ligands, which results in the emissive $T_1$ state being a charge-transfer state that intimately involves orbitals from the L^X ligand. This feature leads to rich photophysical behavior, but none of the reported compounds exhibit exceptional photoluminescence quantum yields, particularly those that luminesce in the red region.

We reasoned that these L^X ligand classes are ideally suited to support efficient red phosphorescence when paired with C^N ligands designed to engender phosphorescence in that region. In this case, the emissive charge-transfer state would involve the C^N ligand, as it most often does, but the electron-rich salicylaldime or 2-picolinamide would influence the Ir 5d $\pi$ orbital energy, excited-state SOC, and excited-state dynamics, as we have seen with other classes of electron-rich L^X ligands.[31,46] In the present work, we adopt two complementary classes of L^X ligands, *N*-substituted salicylaldimine ($\mathbf{L^1}$ and $\mathbf{L^2}$) and *N*-substituted 2-picolinamide ($\mathbf{L^3}$−$\mathbf{L^5}$), to design high-performing red emitters. In the former, the imine "L" functionality is tuned via substituent modification, and in the latter, it is the amide "X" functionality, and both modifications serve the ultimate goal of optimizing red phosphorescence. A common cyclometalating ligand, 1-phenylisoquinoline (piq), which is known to produce red phosphorescence, was paired with all of the L^X ligands. The two best-performing ancillary ligands ($\mathbf{L^1}$ and $\mathbf{L^5}$) were also used with 1-phenylisoquinoline-4-carbonitrile (CNpiq) to evaluate their efficacy in the deep-red region. In total, seven new red-emitting complexes have been reported, with all of them exhibiting exceptionally high photoluminescence quantum yields that rival or exceed those of previous generations. A detailed description of the electrochemical and photophysical properties evaluates the influence of the ancillary ligands on these compounds. This study shows that salicylaldimine and picolinamide ancillary ligands can support red and deep-red phosphors with exceptional $\Phi_{PL}$ values, making them attractive targets for the design of red emitters used in OLED devices and other optoelectronic applications.

## EXPERIMENTAL SECTION

**Materials.** Reactions were performed by using standard Schlenk techniques. Toluene for photophysical measurements and tetrahydrofuran (THF) and acetonitrile for electrochemical measurements were obtained from a Grubbs Solvent Purification System and deaerated with argon. Tetrabutylammonium hexafluorophosphate ($TBAPF_6$) was recrystallized from hot ethanol, and ferrocene was purified by sublimation before use in cyclic voltammetry experiments. Commercially available starting materials and reagents were used without further purification. The iridium dimers of the general formula $[Ir(C^N)_2(\mu\text{-}Cl)]_2$ (C^N = cyclometalating ligand) were prepared by following literature procedures.[47] Salicylaldimine ligands $\mathbf{L^1H}$ and $\mathbf{L^2H}$ were prepared using the classic Schiff base synthesis route.[48,49] Picolinamide ligands $\mathbf{L^3H}$−$\mathbf{L^5H}$ were synthesized by coupling pyridine-2-carbonyl chloride hydrochloride with the corresponding amines.[50,51]

**Physical Methods.** $^1H$ and $^{13}C\{^1H\}$ NMR spectra (Figures S1−S14) were collected at room temperature using a JEOL ECA-500 or ECA-600 NMR spectrometer. The ESI-MS experiments (Figures S15−S21) were carried out at The University of Texas at Austin's Mass Spectrometry Facility or Texas A&M University Chemistry Department Mass Spectrometry Facility. UV−vis absorption spectra were recorded in toluene solutions in 1 cm screw-capped quartz cuvettes using an Agilent Cary 8454 UV−vis spectrophotometer. Emission spectra were measured using a Horiba FluoroMax-4 spectrofluorometer with appropriate long-pass filters to exclude stray excitation light from detection. Samples for emission spectra were prepared in a nitrogen-filled glovebox using dry, deoxygenated solvents to exclude air. Emission quantum yields were determined relative to the standard of tetraphenylporphyrin (TPP) in toluene, which has a reported fluorescence quantum yield ($\Phi_F$) of 0.11. Thin-film PMMA samples were kept under nitrogen until immediately before measurement. Low-temperature measurements were performed with a custom quartz EPR tube with high-vacuum Teflon valve seals and cooled to 77 K in liquid nitrogen using a finger Dewar. The absolute quantum yields of complexes doped into poly(methyl methacrylate) (PMMA) thin films were measured by using a Spectralon-coated integrating sphere integrated with a Horiba FluoroMax-4 spectrofluorometer. Luminescence lifetimes were measured on a Horiba DeltaFlex Lifetime System, using appropriate pulsed diode excitation. Cyclic voltammetry (CV) measurements were carried out with a CH Instruments 602E potentiostat using a three-electrode system, interfaced with a nitrogen glovebox via wire feedthroughs. Measurements were performed in acetonitrile or THF solutions with 0.1 M $TBAPF_6$ as a supporting electrolyte, by using a 3 mm diameter glassy carbon working electrode, Pt wire counter electrode, and silver wire pseudoreference electrode. All potentials displayed in this work were referenced to an internal standard of ferrocene.

**PMMA Film Fabrication.** A solution of PMMA (98 mg, 35 kDa) in dichloromethane (1.0 mL) was prepared at room temperature in a nitrogen-filled glovebox. Then, the respective iridium complex (2 mg, 2 wt %) was added to the solution and stirred, giving a homogeneous solution. The resulting solution was drop-coated on a quartz substrate and dried at room temperature for 24 h.

**X-ray Crystallography Details.** Single crystals were mounted on a Bruker Apex II three-circle diffractometer using Mo K$\alpha$ radiation ($\lambda$ = 0.71073 Å). The data was collected at 123(2) K, then processed and refined within the APEXII software. Structures were solved by intrinsic phasing methods in SHELXT and refined by standard difference Fourier techniques in the program SHELXL.[52] Hydrogen atoms bonded to carbon were placed in calculated positions using the standard riding model and refined isotropically; all non-hydrogen atoms were refined anisotropically. The structure of **piq-L²** included heavily disordered solvent electron density that could not be satisfactorily refined, necessitating the use of the SQUEEZE command in PLATON.[53] The structure of **piq-L⁵** included two disordered solvent molecules. Distance restraints (SADI) and rigid-bond restraints (SIMU and DELU) are used to restrain the


https://doi.org/10.1021/acs.inorgchem.3c01770
Inorg. Chem. 2023, 62, 11278−11286

disordered parts. Crystallographic details are summarized in Tables S1 and S2.

**General Procedure for Preparation of Salicylaldimine Complexes.** The chloro-bridged cyclometalated iridium dimer was treated with 5 equiv of $Na_2CO_3$ in 10 mL of ethanol and stirred for 1 h, and then 2.1 equiv of the salicylaldimine ligand ($\mathbf{L}^n\mathbf{H}$, $n$ = 1 or 2) was added. The reaction mixture was refluxed overnight. After the solvent was removed under vacuum, the residue was redissolved in $CH_2Cl_2$ and then filtered through a thin layer of alumina, using $CH_2Cl_2$ as the eluent to flush out the product.

*Preparation of [Ir(piq)$_2$L$^1$] (**piq-L$^1$**).* Prepared by the general procedure using $[Ir(piq)_2(\mu\text{-}Cl)]_2$ (100 mg, 0.079 mmol) and $\mathbf{L}^1\mathbf{H}$ (27 mg, 0.17 mmol). The resulting crude product was further purified by recrystallization from $CH_2Cl_2$/pentane to give a red solid. Yield: 67 mg, 55%. $^1$H NMR (500 MHz, $CDCl_3$) $\delta$ 9.01−8.94 (m, 1H, piq ArH), 8.94−8.86 (m, 1H, ArH), 8.81 (d, $J$ = 6.4 Hz, 1H, ArH), 8.36 (d, $J$ = 6.4 Hz, 1H, ArH), 8.21 (d, $J$ = 8.0 Hz, 1H, ArH), 8.12 (d, $J$ = 8.0 Hz, 1H, ArH), 8.04 (s, 1H, N = CHAr), 7.96−7.90 (m, 1H, ArH), 7.88−7.80 (m, 1H, ArH), 7.74−7.70 (m, 2H, ArH), 7.68−7.64 (m, 2H, ArH), 7.44 (d, $J$ = 6.4 Hz, 1H, ArH), 7.29 (d, $J$ = 6.3 Hz, 1H, ArH), 7.14 (t, $J$ = 6.8 Hz, 1H, ArH), 7.07 (d, $J$ = 7.9 Hz, 1H, ArH), 6.94−6.85 (m, 2H, ArH), 6.71−6.58 (m, 3H, ArH), 6.42 (d, $J$ = 6.6 Hz, 1H, ArH), 6.38 (t, $J$ = 7.3 Hz, 1H, ArH), 6.17 (d, $J$ = 7.6 Hz, 1H, ArH), 3.15 (td, $J$ = 10.7, 5.6 Hz, 1H, $CH_2CH_2CH_3$), 2.95 (td, $J$ = 10.6, 5.5 Hz, 1H, $CH_2CH_2CH_3$), 1.21−1.13 (m, 1H, $CH_2CH_2CH_2CH_3$), 1.00−0.90 (m, 1H, $CH_2CH_2CH_2CH_3$), 0.30 (t, $J$ = 7.3 Hz, 3H, $CH_2CH_2CH_3$). $^{13}$C{$^1$H} NMR (126 MHz, $CDCl_3$) $\delta$: 170.1, 169.1, 166.3, 162.0, 156.3, 155.3, 146.4, 146.3, 141.6, 141.2, 137.2, 136.8, 134.7, 134.2, 133.4, 132.2, 130.7, 130.6, 129.94, 129.87, 129.3, 129.2, 127.8, 127.6, 127.5, 127.4, 127.0, 126.7, 126.5, 126.3, 124.4, 121.4, 120.9, 120.1, 119.9, 119.5, 112.8, 65.7, 24.5, 11.2. HRMS-ESI ($m/z$): $[M + H]^+$ calcd for $C_{40}H_{32}IrN_3O$, 764.2250; found, 764.2238.

*Preparation of [Ir(piq)$_2$L$^2$] (**piq-L$^2$**).* Prepared by the general procedure using $[Ir(piq)_2(\mu\text{-}Cl)]_2$ (100 mg, 0.079 mmol) and $\mathbf{L}^2\mathbf{H}$ (35 mg, 0.17 mmol). The resulting crude product was further purified by recrystallization from $CH_2Cl_2$/pentane to give a red solid. The compound was isolated as a dichloromethane solvate, **piq-L$^2$**·$0.5CH_2Cl_2$. Yield: 75 mg, 56%. $^1$H NMR (500 MHz, $CDCl_3$) $\delta$ 9.01−8.92 (m, 1H, ArH), 8.86 (d, $J$ = 6.3 Hz, 1H, ArH), 8.78 (d, $J$ = 6.4 Hz, 1H, ArH), 8.54 (d, $J$ = 8.5 Hz, 1H, ArH), 8.18 (d, $J$ = 8.0 Hz, 1H, ArH), 8.07 (s, 1H, N═CHAr), 7.90 (d, $J$ = 7.9 Hz, 1H, ArH), 7.88−7.83 (m, 1H, ArH), 7.72−7.57 (m, 5H, ArH), 7.45 (d, $J$ = 6.3 Hz, 1H, ArH), 7.35 (d, $J$ = 6.4 Hz, 1H, ArH), 7.15 (t, $J$ = 6.8 Hz, 1H, ArH), 7.08 (d, $J$ = 8.0 Hz, 1H, ArH), 6.91 (t, $J$ = 7.6 Hz, 1H, ArH), 6.68 (t, $J$ = 7.4 Hz, 1H, ArH), 6.65−6.58 (m, 2H, ArH), 6.43 (t, $J$ = 6.8 Hz, 1H, ArH), 6.40−6.31 (m, 4H, ArH), 6.20 (d, $J$ = 7.6 Hz, 1H, ArH), 5.93 (d, $J$ = 7.9 Hz, 2H, ArH), 2.05 (s, 3H, $ArCH_3$). $^{13}$C{$^1$H} NMR (126 MHz, $CDCl_3$) $\delta$: 169.8, 169.4, 167.4, 161.7, 155.8, 155.1, 149.5, 146.3, 145.9, 142.0, 140.9, 137.0, 136.8, 135.2, 134.14, 134.07, 133.8, 133.2, 130.6, 130.5, 129.9, 129.5, 129.3, 128.8, 127.9, 127.7, 127.4, 127.3, 127.2, 127.1, 126.8, 126.6, 126.1, 124.9, 122.2, 121.9, 120.5, 119.8, 119.7, 119.3, 113.3, 21.6. HRMS-ESI ($m/z$): $[M + H]^+$ calcd for $C_{44}H_{32}IrN_3O$, 812.2250; found, 812.2237.

*Preparation of [Ir(CNpiq)$_2$L$^1$] (**CNpiq-L$^1$**).* Prepared by the general procedure using $[Ir(CNpiq)_2(\mu\text{-}Cl)]_2$ (25 mg, 0.020 mmol) and $\mathbf{L}^1\mathbf{H}$ (7 mg, 0.043 mmol). The resulting crude product was further purified by recrystallization from THF/pentane to give a purple solid. The compound was isolated as a tetrahydrofuran solvate, **CNpiq-L$^1$**·0.5THF. Yield: 13 mg, 38%. $^1$H NMR (600 MHz, $CD_2Cl_2$) $\delta$ 9.08 (s, 1H, ArH), 9.02 (d, $J$ = 8.5 Hz, 1H, ArH), 8.92 (d, $J$ = 8.5 Hz, 1H, ArH), 8.63 (s, 1H, ArH), 8.30 (t, $J$ = 8.8 Hz, 2H, ArH), 8.18 (t, $J$ = 8.9 Hz, 2H, ArH), 8.04 (s, 1H, N═CHAr), 7.97−7.86 (m, 3H, ArH), 7.84 (t, $J$ = 7.7 Hz, 1H, ArH), 7.14−7.08 (m, 2H, ArH), 7.00 (q, $J$ = 7.0 Hz, 2H, ArH), 6.74 (q, $J$ = 8.0 Hz, 2H, ArH), 6.58 (d, $J$ = 7.6 Hz, 1H, ArH), 6.49 (d, $J$ = 9.0 Hz, 1H, ArH), 6.40 (t, $J$ = 7.4 Hz, 1H, ArH), 6.16 (d, $J$ = 7.6 Hz, 1H, ArH), 3.16 (td, $J$ = 10.7, 5.4 Hz, 1H, $CH_2CH_2CH_3$), 2.98 (td, $J$ = 10.6, 5.5 Hz, 1H, $CH_2CH_2CH_3$), 1.17−1.08 (m, 1H, $CH_2CH_2CH_2CH_3$), 0.96−0.87 (m, 1H, $CH_2CH_2CH_2CH_3$), 0.33 (t, $J$ = 7.3 Hz, 3H, $CH_2CH_2CH_3$). $^{13}$C{$^1$H} NMR (151 MHz, $CDCl_3$) $\delta$: 175.0, 174.3, 166.3, 163.2, 159.2, 158.5, 147.1, 146.4, 144.5, 144.3, 135.8, 135.3, 134.79, 134.76, 134.3, 133.5, 133.3, 132.3, 132.2, 132.1, 131.4, 131.0, 129.4, 129.2, 128.4, 127.8, 125.2, 125.1, 125.0, 124.4, 123.6, 121.9, 121.1, 120.8, 115.6, 115.2, 114.2, 103.9, 102.9, 65.3, 24.7, 11.2. HRMS-ESI ($m/z$): $[M + H]^+$ calcd for $C_{42}H_{30}IrN_5O$, 814.2155; found, 814.2144.

**General Procedure for Preparation of Picolinamide Complexes.** After 2.5 equiv of the picolinamide ligand ($\mathbf{L}^n\mathbf{H}$, $n$ = 3−5) were treated with 3 equiv of sodium methoxide in 10 mL of anhydride methanol and stirred for 10 min, 1 equiv of chloro-bridged cyclometalated iridium dimer was added. The reaction mixture was refluxed overnight. After the solvent was removed under vacuum, the residue was redissolved in $CH_2Cl_2$ and then filtered through a thin layer of alumina. After the solvent had evaporated, the crude product was purified by column chromatography on silica gel, using $CH_2Cl_2$ as the eluent.

*Preparation of [Ir(piq)$_2$L$^3$] (**piq-L$^3$**).* Prepared by the general procedure using $[Ir(piq)_2(\mu\text{-}Cl)]_2$ (100 mg, 0.079 mmol) and $\mathbf{L}^3\mathbf{H}$ (33 mg, 0.20 mmol) to give a red solid. Yield: 71 mg, 59%. $^1$H NMR (500 MHz, $CD_2Cl_2$) $\delta$ 9.00−8.91 (m, 2H, ArH), 8.58 (d, $J$ = 6.3 Hz, 1H, ArH), 8.25 (m, 3H, ArH), 7.93−7.89 (m, 2H, ArH), 7.81 (t, $J$ = 7.5 Hz, 1H, ArH), 7.77−7.69 (m, 4H, ArH), 7.54 (d, $J$ = 4.8 Hz, 1H, ArH), 7.50 (d, $J$ = 6.5 Hz, 1H, ArH), 7.47 (d, $J$ = 6.5 Hz, 1H, ArH), 7.31 (d, $J$ = 6.3 Hz, 1H, ArH), 7.11 (t, $J$ = 6.2 Hz, 1H, ArH), 7.04 (t, $J$ = 7.5 Hz, 1H, ArH), 6.99 (t, $J$ = 7.5 Hz, 1H, ArH), 6.82 (t, $J$ = 7.2 Hz, 1H, ArH), 6.74 (t, $J$ = 7.3 Hz, 1H, ArH), 6.35 (d, $J$ = 7.4 Hz, 1H, ArH), 6.30 (d, $J$ = 7.5 Hz, 1H, ArH), 3.37 (td, J = 10.2, 6.2 Hz, 1H, $CH_2CH_2CH_3$), 2.89 (td, J = 10.4, 4.6 Hz, 1H, $CH_2CH_2CH_3$), 1.10−0.99 (m, 1H, $CH_2CH_2CH_2CH_3$), 0.65−0.59 (m, 1H, $CH_2CH_2CH_2CH_3$), 0.29 (t, $J$ = 7.2 Hz, 3H, $CH_2CH_2CH_3$). $^{13}$C{$^1$H} NMR (126 MHz, $CD_2Cl_2$) $\delta$: 170.4, 169.8, 169.2, 160.5, 157.7, 157.5, 148.5, 146.7, 145.5, 142.1, 141.0, 137.3, 136.8, 136.5, 132.6, 132.2, 131.0, 130.8, 130.5, 130.1, 129.6, 128.0, 127.9, 127.28, 127.25, 126.9, 126.3, 126.2, 126.1, 120.9, 120.7, 120.5, 120.4, 49.1, 23.0, 11.6. HRMS-ESI ($m/z$): $[M + H]^+$ calcd for $C_{39}H_{31}IrN_4O$, 765.2202; found, 765.2198.

*Preparation of [Ir(piq)$_2$L$^4$] (**piq-L$^4$**).* Prepared by the general procedure using $[Ir(piq)_2(\mu\text{-}Cl)]_2$ (100 mg, 0.079 mmol) and $\mathbf{L}^4\mathbf{H}$ (42 mg, 0.20 mmol) to give a red solid. Yield: 64 mg, 50%. $^1$H NMR (500 MHz, $CDCl_3$) $\delta$ 9.03 (d, $J$ = 6.4 Hz, 1H, ArH), 8.93 (d, $J$ = 8.9 Hz, 1H, ArH), 8.65 (d, $J$ = 8.5 Hz, 1H, ArH), 8.39 (d, $J$ = 8.2 Hz, 1H, ArH), 8.22 (d, $J$ = 8.0 Hz, 1H, ArH), 7.99−7.56 (m, 9H, ArH), 7.50 (d, $J$ = 5.2 Hz, 1H, ArH), 7.45 (d, $J$ = 6.5 Hz, 1H, ArH), 7.28−7.23 (m, 1H, ArH), 7.15 (t, $J$ = 7.4 Hz, 1H, ArH), 7.00 (t, $J$ = 7.4 Hz, 1H, ArH), 6.80 (t, $J$ = 7.4 Hz, 1H, ArH), 6.70 (t, $J$ = 7.4 Hz, 1H, ArH), 6.52 (d, $J$ = 7.7 Hz, 1H, ArH), 6.48 (t, $J$ = 7.4 Hz, 1H, ArH), 6.40 (d, $J$ = 8.0 Hz, 2H, ArH), 6.25 (d, $J$ = 8.3 Hz, 2H, ArH), 6.00 (d, $J$ = 7.7 Hz, 1H, ArH), 2.01 (s, 3H, $ArCH_3$). $^{13}$C{$^1$H} NMR (126 MHz, $CDCl_3$) $\delta$: 170.1, 169.8, 169.6, 159.0, 157.5, 156.9, 148.4, 146.5, 144.9, 144.4, 142.5, 141.0, 137.2, 136.9, 136.5, 133.3, 131.9, 131.3, 131.0, 130.8, 130.5, 130.2, 129.8, 129.3, 128.0, 127.9, 127.6, 127.4, 127.32, 127.26, 127.1, 127.0, 126.8, 126.3, 126.2, 124.8, 121.0, 120.7, 120.2, 120.1, 20.9. HRMS-ESI ($m/z$): $[M + H]^+$ calcd for $C_{43}H_{31}IrN_4O$, 813.2202; found, 813.2185.

*Preparation of [Ir(piq)$_2$L$^5$] (**piq-L$^5$**).* Prepared by the general procedure using $[Ir(piq)_2(\mu\text{-}Cl)]_2$ (100 mg, 0.079 mmol) and $\mathbf{L}^5\mathbf{H}$ (53 mg, 0.20 mmol) to give a red solid. Yield: 86 mg, 63%. $^1$H NMR (600 MHz, $CDCl_3$) $\delta$ 8.98−8.93 (m, 2H, ArH), 8.55 (d, $J$ = 8.5 Hz, 1H, ArH), 8.39 (d, $J$ = 7.7 Hz, 1H, ArH), 8.24 (d, $J$ = 7.8 Hz, 1H, ArH), 7.94−7.90 (m, 1H, ArH), 7.88−7.82 (m, 2H, ArH), 7.78−7.67 (m, 4H, ArH), 7.64 (t, $J$ = 7.1 Hz, 1H, ArH), 7.60 (d, $J$ = 6.4 Hz, 1H, ArH), 7.54 (d, $J$ = 5.3 Hz, 1H, ArH), 7.46 (d, $J$ = 6.4 Hz, 1H, ArH), 7.28 (d, $J$ = 6.4 Hz, 1H, ArH), 7.19 (t, $J$ = 5.7 Hz, 1H, ArH), 7.03 (t, $J$ = 6.9 Hz, 1H, ArH), 6.84−6.77 (m, 3H, ArH), 6.71 (t, $J$ = 6.9 Hz, 1H, ArH), 6.56 (d, $J$ = 6.4 Hz, 1H, ArH), 6.52 (t, $J$ = 6.9 Hz, 1H, ArH), 6.45 (d, $J$ = 8.2 Hz, 2H, ArH), 6.01 (d, $J$ = 6.3 Hz, 1H, ArH). $^{13}$C{$^1$H} NMR (126 MHz, $CDCl_3$) $\delta$: 170.3, 169.7, 169.4, 157.9, 156.2, 148.6, 146.4, 144.9, 142.2, 140.8, 137.4, 136.9, 136.5, 133.4, 131.8, 131.2, 131.0, 130.6, 130.3, 129.8, 129.5, 128.2, 127.0, 127.4, 127.4, 127.2, 127.2, 127.0, 126.3, 126.1, 125.4, 124.34, 124.31, 121.2, 120.7, 120.6, 120.5. HRMS-ESI ($m/z$): $[M + H]^+$ calcd for $C_{43}H_{28}F_3IrN_4O$, 867.1917; found, 867.1906.



https://doi.org/10.1021/acs.inorgchem.3c01770
Inorg. Chem. 2023, 62, 11278−11286

*Preparation of [Ir(CNpiq)$_2$L$^5$] (**CNpiq-L$^5$**).* Prepared by the general procedure using [Ir(CNpiq)$_2$($\mu$-Cl)]$_2$ (30 mg, 0.022 mmol) and **L$^5$H** (15 mg, 0.056 mmol) to give a red solid. Yield: 13 mg, 64%. $^1$H NMR (500 MHz, $CDCl_3$) $\delta$ 9.27 (s, 1H, Ar*H*), 8.99 (d, J = 9.6 Hz, 1H,, Ar*H*), 8.48 (t, J = 7.8 Hz, 2H, Ar*H*), 8.33 (d, J = 8.1 Hz, 1H, Ar*H*), 8.28 (d, J = 8.1 Hz, 1H, Ar*H*), 8.25 (d, J = 8.3 Hz, 1H, Ar*H*), 8.00−7.94 (m, 2H, Ar*H*), 7.94−7.89 (m, 2H, Ar*H*), 7.81 (t, *J* = 7.8 Hz, 1H, Ar*H*), 7.75 (d, J = 8.1 Hz, 1H, Ar*H*), 7.48 (d, J = 4.6 Hz, 1H, Ar*H*), 7.31 (t, *J* = 7.0 Hz, 1H, Ar*H*), 7.14 (t, *J* = 8.3 Hz, 1H, Ar*H*), 6.94 (td, J = 7.4, 1.2 Hz, 1H, Ar*H*), 6.85−6.78 (m, 3H, Ar*H*), 6.69−6.60 (m, 2H, Ar*H*), 6.42 (d, J = 8.2 Hz, 2H, Ar*H*), 6.03 (d, *J* = 6.5 Hz, 1H, Ar*H*). $^{13}$C{$^1$H} NMR (126 MHz, $CD_2Cl_2$) $\delta$: 174.8, 174.0, 149.1, 146.9, 135.0, 134.0, 133.7, 133.6, 132.8, 132.2, 132.0, 131.9, 131.4, 130.4, 129.8, 128.2, 125.9, 124.7, 124.3, 124.2, 122.1, 121.3, 114.4. HRMS-ESI (*m*/*z*): [M + H]$^+$ calcd for $C_{45}H_{26}F_3IrN_6O$, 917.1822; found, 917.1823.

## RESULTS AND DISCUSSION

**Synthesis and Structural Characterization.** The synthesis of seven new heteroleptic bis-cyclometalated iridium complexes is outlined in Scheme 1. The substituted

**Scheme 1. Synthesis of Target Complexes**

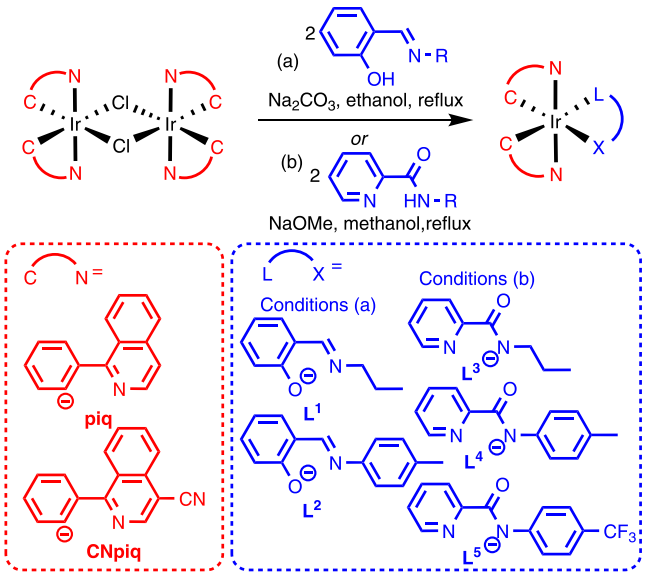


Compounds studied and isolated yields:
**piq-L$^1$** (55%), **piq-L$^2$** (56%), **CNpiq-L$^1$** (38%)
**piq-L$^3$** (59%), **piq-L$^4$** (50%), **piq-L$^5$** (63%), **CNpiq-L$^5$** (64%)

salicylaldimine complexes were prepared by treating [Ir(C^N)$_2$($\mu$-Cl)]$_2$ with the corresponding salicylaldimine proligand (**L$^1$H** or **L$^2$H**) and sodium carbonate in ethanol under reflux in an ambient atmosphere. The synthesis of the 2-picolinamide complexes started by treating the 2-picolinamide proligand (**L$^3$H**−**L$^5$H**) with sodium methoxide in methanol at room temperature. The resultant deprotonated ligand was then combined with the chloro-bridged cyclometalated iridium dimer and refluxed overnight to give the target complexes. The compounds are stable to chromatographic purification, which was used along with recrystallization for purification, and isolated in moderate to good yields ranging from 38%−64%. Their identities and purity are validated by high-resolution ESI-MS and $^1$H and $^{13}$C{$^1$H} NMR spectroscopy (Figures S1−S14). The NMR spectra of all new compounds are consistent with the $C_1$ symmetry. Compounds are denoted with the formalism **C^N-L$^n$**, where **C^N** indicates the cyclometalating ligand, **piq** for 1-phenylisoquinoline, or **CNpiq** for 1-phenylisoquinoline-4-carbonitrole, and **L$^n$** is the numerical designation for the ancillary ligand, as described in Scheme 1.

All five of the C^N = piq complexes were characterized by single-crystal X-ray diffraction to confirm the coordination environment, and their molecular structures are shown in Figures 1 and 2 with refinement data summarized in Tables S1

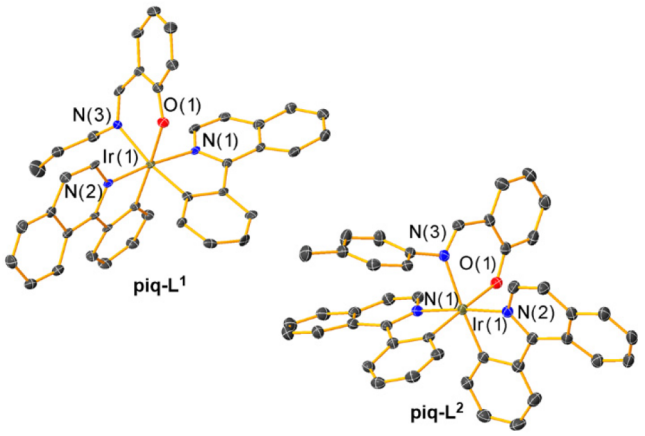


**Figure 1.** Molecular structures of salicylaldimine complexes **piq-L$^1$** and **piq-L$^2$**, determined by single-crystal X-ray diffraction. Thermal ellipsoids are shown at the 50% probability level. Hydrogen atoms have been omitted for clarity.

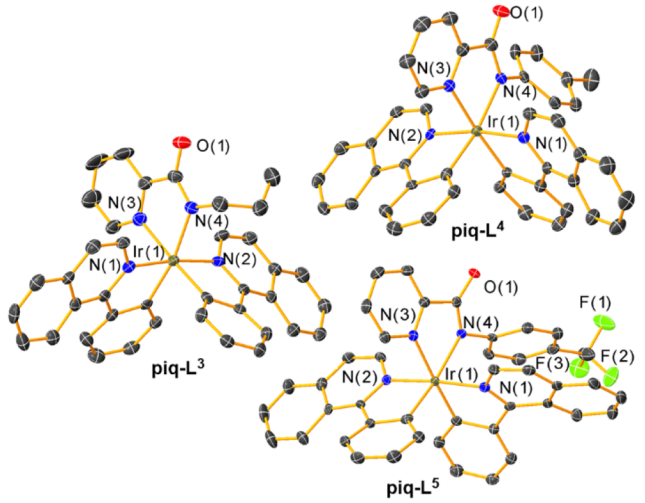


**Figure 2.** Molecular structures of 2-picolinamide complexes **piq-L$^3$**, **piq-L$^4$**, and **piq-L$^5$**, determined by single-crystal X-ray diffraction. Thermal ellipsoids are shown at the 50% probability level. Hydrogen atoms and solvent molecules have been omitted for clarity.

and S2 of the Supporting Information. In the salicylaldimine complexes (**piq-L$^1$** and **piq-L$^2$**, Figure 1), the ancillary ligand C−O bond distances are ca. 1.30 Å, shorter than a typical C−O single bond (ca. 1.4 Å), and indicative of some $\pi$-delocalization into the ancillary ligand core. However, in the picolinamide ligands in complexes **piq-L$^3$**, **piq-L$^4$**, and **piq-L$^5$** (Figure 2), while there is evidence for delocalization of the amide nitrogen atom's negative charge into the adjacent C═O bond, there is no delocalization of charge into the pyridine "L" donor arm. Specifically, the C−C distance from the 2-position of the pyridine ring to the amide C═O carbon ranges from


https://doi.org/10.1021/acs.inorgchem.3c01770
Inorg. Chem. 2023, 62, 11278−11286

1.492(6) to 1.514(6) Å, consistent with a C−C single bond with no $\pi$-delocalization. Moreover, the structures in Figure 2 demonstrate the *N,N* binding mode of the 2-picolinamide ligand, as opposed to the *N,O* binding mode we observed with other amidate ligands that lack the pyridine ring.[46] The X−Ir−N (X = O or N) bite angles are very similar in the two six-member chelate salicylaldimine complexes, 86.3(3)° and 87.14(8)°, and, as expected, smaller in the five-member chelate 2-picolinamide complexes, ranging from 75.88(14)° to 76.28(16)°.

**Electrochemistry.** The electrochemical properties of the complexes were studied by cyclic voltammetry in anaerobic acetonitrile (salicylaldimine complexes) or THF (2-picolinamide complexes) solutions. The overlaid voltammograms are shown in Figure 3, with the redox potentials reported relative

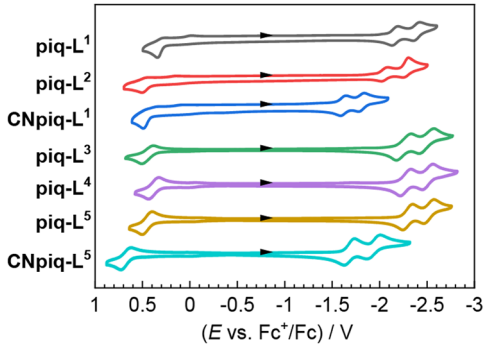


**Figure 3.** Cyclic voltammograms of all complexes, recorded in acetonitrile ($\mathbf{L^1}$ and $\mathbf{L^2}$ complexes) or THF ($\mathbf{L^3}$–$\mathbf{L^5}$ complexes) with 0.1 M $TBAPF_6$ electrolyte. Currents are normalized to bring all the traces into the same scale, and the arrows indicate the scan direction.

**Table 1. Summary of Redox Potentials for All Complexes Measured by Cyclic Voltammetry**[a]

| | $E^{ox}$/V | $E^{red}$/V | $\Delta E_{H-L}$[c]/eV |
|---|---|---|---|
| **piq-L$^1$** | 0.30[b] | −2.17, −2.39 | 2.47 |
| **piq-L$^2$** | 0.45[b] | −2.06, −2.29 | 2.51 |
| **CNpiq-L$^1$** | 0.44[b] | −1.62, −1.81 | 2.06 |
| **piq-L$^3$** | 0.45 | −2.25, −2.50 | 2.70 |
| **piq-L$^4$** | 0.38 | −2.28, −2.51 | 2.66 |
| **piq-L$^5$** | 0.46 | −2.29, −2.52 | 2.75 |
| **CNpiq-L$^5$** | 0.68 | −1.68, −1.94 | 2.36 |

[a]Experiments were conducted in MeCN for salicylaldimine complexes ($\mathbf{L^1}$ and $\mathbf{L^2}$) and THF for 2-picolinamide complexes ($\mathbf{L^3}$–$\mathbf{L^5}$). Potentials are referenced to the $Fc^+$/Fc couple. [b]Irreversible wave; the half-peak potential[54] is reported. [c]Electrochemical HOMO−LUMO gap, estimated as $E^{ox} - E^{red}$.

to the ferrocene couple ($Fc^+$/Fc) and summarized in Table 1. Two reversible one-electron reduction waves are observed in all the complexes, which depend slightly on the ancillary ligand and are assigned to the subsequent reduction of each C^N ligand. Complexes with the more-conjugated cyclometalating ligand CNpiq have reduction potentials that are >500 mV more positive than the piq analogues with the same ancillary ligand, suggesting substantial stabilization of the LUMO energy brought on by the cyano group.[34]

The formal $Ir^{IV}/Ir^{III}$ couple, $E^{ox}$, is responsive to ancillary ligand substitution. In the salicylaldimine complexes with C^N = piq, replacing the *N*-propyl substituent in **piq-L$^1$** with an *N*-tolyl substituent in **piq-L$^2$** induces a significant 150-mV positive shift in $E^{ox}$. In the 2-picolinamide series, $E^{ox}$ is less responsive to the *N*-substituent, and for reasons that are unclear, replacing *N*-propyl (**piq-L$^3$**) with *N*-tolyl (**piq-L$^4$**) causes a shift in the opposite direction, toward a more negative potential. The $CF_3$ group in **piq-L$^5$** has the expected effect of anodically shifting $E^{ox}$. The $E^{ox}$ value also experiences a significant positive shift in the CNpiq complexes, at parity of the ancillary ligand, suggesting that there is some delocalization of the HOMO density onto the C^N ligand. For the five C^N = piq complexes, the electrochemical HOMO−LUMO gaps ($\Delta E_{H-L}$), estimated from the difference between $E^{ox}$ and the first $E^{red}$ potential, are all similar for a given L^X ligand class. Those with 2-picolinamide ancillary ligands have larger $\Delta E_{H-L}$ values than the salicylaldimine versions, but within a given class, the HOMO−LUMO gaps vary by no more than 90 mV. The bigger change in $\Delta E_{H-L}$ comes about in the CNpiq complexes, where the large LUMO stabilization results in a smaller HOMO−LUMO (H−L) gap, though again the 2-picolinamide complex **CNpiq-L$^5$** has a larger $\Delta E_{H-L}$ than the salicylaldimine complex **CNpiq-L$^1$**.

**Photophysical Properties.** UV−vis absorption spectra were recorded at room temperature in toluene and are overlaid in Figure 4.

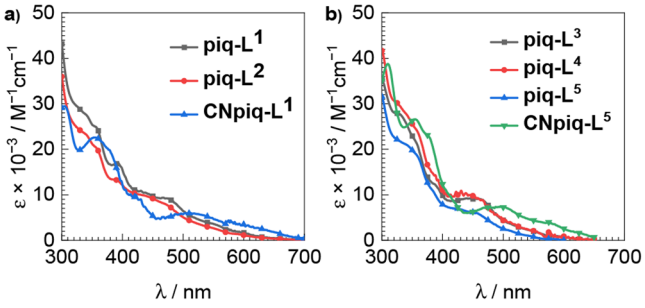


**Figure 4.** Overlaid UV−vis absorption spectra of a) salicylaldimine complexes and b) 2-picolinamide complexes, recorded in toluene at room temperature.

There are no unexpected features in the spectra, which align well with other well-characterized bis-cyclometalated iridium complexes.[29,30] The absorption bands in the UV region ($\lambda$ < 350 nm) are dominated by intense spin-allowed ligand-centered $\pi \rightarrow \pi^*$ transitions involving cyclometalating and ancillary ligands. The less intense, overlapping absorption bands tailing beyond 600 nm are assigned to singlet and triplet metal-to-ligand charge transfer ($^1$MLCT/$^3$MLCT) transitions. Consistent with their smaller electrochemical HOMO−LUMO gaps, these bands tail to longer wavelengths in the CNpiq complexes. In the piq series, the ancillary ligand structure and substitution have little impact on UV−vis absorption features.

Figure 5 collects the room-temperature photoluminescence spectra of the iridium complexes, and Table 2 summarizes the data. The excitation spectra are shown in the Supporting Information (Figures S22−S28) and in each case overlay perfectly with UV−vis absorption spectra, indicating that there are no impurities interfering with the observed emission. Time-resolved photoluminescence measurements, used to determine PL lifetimes, are collected in Figures S31−S44. Consistent with the electrochemical HOMO−LUMO gaps (Table 1), the peak emission wavelengths in the piq-salicylaldimine series (**piq-L$^1$**


https://doi.org/10.1021/acs.inorgchem.3c01770
Inorg. Chem. 2023, 62, 11278−11286

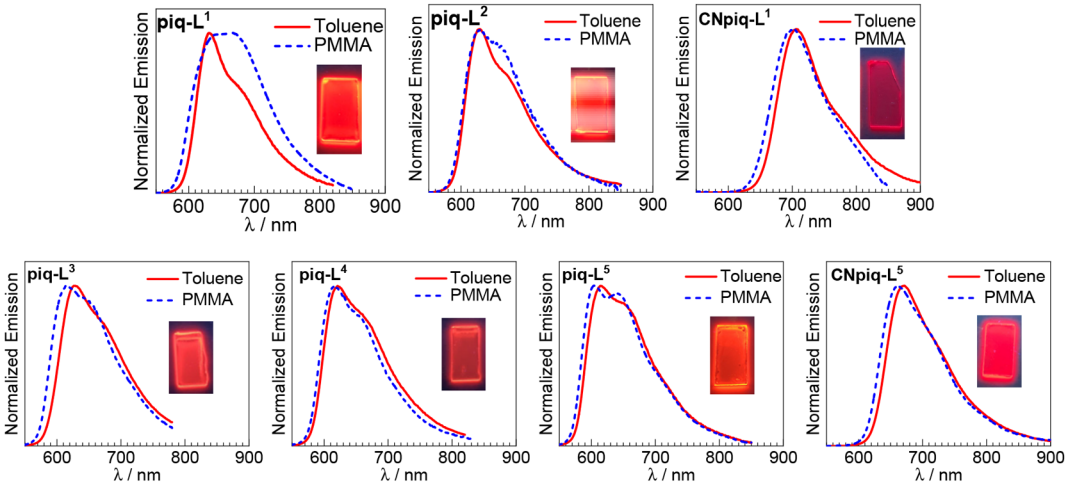


**Figure 5.** Overlaid photoluminescence spectra of all complexes recorded at room temperature. The emission spectra were recorded in both toluene (red solid line) and as a 2 wt % transparent PMMA film (blue dashed line). The inset shows a photograph of the PMMA film.

**Table 2. Summary of Photoluminescence Data for All Complexes**

| | Toluene | | | | 2 wt % in PMMA | | | |
|---|---|---|---|---|---|---|---|---|
| | $\lambda$/nm | $\Phi_{PL}$ | $\tau/\mu s$ | $(k_r \times 10^{-5}\ /s^{-1})/(k_{nr} \times 10^{-5}\ /s^{-1})$ | $\lambda$/nm | $\Phi_{PL}$ | $\tau/\mu s$ | $(k_r \times 10^{-5}\ /s^{-1})/(k_{nr} \times 10^{-5}\ /s^{-1})$ |
| **piq-L$^1$** | 629, 676(sh) | 0.59 | 1.1 | 5.4/3.7 | 631, 676(sh) | 0.93 | 1.1 | 8.5/0.64 |
| **piq-L$^2$** | 632, 682(sh) | 0.21 | 0.41 | 5.1/19 | 631, 667(sh) | 0.59 | 1.2 | 4.9/3.4 |
| **CNpiq-L$^1$** | 704 | 0.48 | 0.48 | 10/11 | 700 | 0.65 | 0.67 | 9.7/5.2 |
| **piq-L$^3$** | 627, 674(sh) | 0.45 | 1.3 | 3.5/4.2 | 615, 658(sh) | 0.74 | 2.3 | 3.2/1.1 |
| **piq-L$^4$** | 621, 672(sh) | 0.22 | 0.45 | 4.9/17 | 616, 661(sh) | 0.79 | 1.9 | 4.2/1.1 |
| **piq-L$^5$** | 614, 659(sh) | 0.80 | 1.6 | 5.0/1.3 | 604, 643(sh) | 0.65 | 2.0 | 3.3/1.8 |
| **CNpiq-L$^5$** | 672, 728(sh) | 0.76 | 0.90 | 8.4/2.7 | 661, 718(sh) | 0.84 | 1.0 | 8.4/1.6 |

and **piq-L$^2$**) are slightly red-shifted compared to those of the picolinamide analogues with the same C^N ligand. These trends are mirrored in spectra recorded at 77 K in rigid toluene glass, where the vibronic structure is better resolved, and peak wavelengths are slightly blue-shifted relative to room-temperature spectra (Figures S29 and S30).

The complex **piq-L$^1$**, with an *n*-propyl-substituted salicylaldimine ancillary ligand, showed strong red luminescence ($\Phi_{PL}$ = 0.59) in fluid toluene solution with an emission maximum of 629 nm and has a near-unity quantum yield when immobilized in poly(methyl methacrylate) (PMMA) film, with $\Phi_{PL}$ = 0.93. Replacing the *N*-propyl substituent with *N*-tolyl in **piq-L$^2$** causes the quantum yield to decrease by about half, both in solution ($\Phi_{PL}$ = 0.21 for **piq-L$^2$**) and in PMMA film ($\Phi_{PL}$ = 0.59 for **piq-L$^2$**). The much shorter lifetime in solution for **piq-L$^2$** ($\tau$ = 0.41 $\mu$s vs 1.1 $\mu$s) indicates a more than 5-fold increase in the nonradiative rate constant ($k_{nr}$) is largely responsible. In PMMA film, the lifetimes of **piq-L$^1$** and **piq-L$^2$** are similar, but again the increase in $k_{nr}$ is the more significant factor for the decrease in $\Phi_{PL}$. Despite the significant differences in the photoluminescence quantum yield and lifetime between these two compounds, the emission peak wavelengths are nearly identical, suggesting the ancillary ligand substituent does not perturb the emission color but can have significant effects on the excited-state dynamics.

Similar ligand substituent effects can be observed in the picolinamide series, particularly for spectra recorded in a fluid solution. *N*-alkyl-substituted **piq-L$^3$** has a solution quantum yield 2× higher than that of *N*-tolyl analogue **piq-L$^4$**, primarily because of a much higher $k_{nr}$ value in the latter. However, replacing the *N*-tolyl group with 4-trifluoromethylphenyl in **piq-L$^5$** leads to the suppression of $k_{nr}$ and the highest solution quantum yield in the series of 0.80. These observations suggest the possibility that $C_{sp3}$–H bond vibrations in the ancillary ligand are involved in nonradiative decay in these compounds, as eliminating those in **piq-L$^5$** produced the lowest $k_{nr}$ and highest $\Phi_{PL}$. In the PMMA film, the three salicylaldimine complexes have quantum yields and lifetimes similar to those of one another, all quite high for the red region ($\Phi_{PL}$ = 0.65–0.79).

To comment in more detail about the $k_r$ and $k_{nr}$ values in the C^N = piq series, we note that all five compounds have similar $k_r$ values in solution, spanning a narrow range of 3.5–5.4 × $10^5$ $s^{-1}$. These values rival or exceed those of other top-performing red-phosphorescent iridium complexes,[19,31,55] but do not seem to be systematically controlled by the ancillary ligand structure. However, in solution, the $k_{nr}$ values span a wide range and seem to depend strongly on the L^X ligand substituents, with *N*-propyl outperforming *N*-tolyl, and the $CF_3$-substituted analogue **piq-L$^5$** performing the best in solution. In PMMA films, the $k_r$ values are generally similar to the solution values, but in all cases, a large suppression of $k_{nr}$ occurs on account of the more rigid matrix.

From the five C^N = piq compounds, we identified salicylaldimine ligand **L$^1$** and 2-picolinamide ligand **L$^5$** as the two best-performing L^X ligands and hypothesized they could also support efficient phosphorescence with significant deep-red ($\lambda$ = 650–700 nm) and near-infrared ($\lambda$ > 700) intensity. To test this, we prepared cyano-substituted analogues **CNpiq-L$^1$** and **CNpiq-L$^5$**, which have smaller HOMO–LUMO gaps


https://doi.org/10.1021/acs.inorgchem.3c01770
Inorg. Chem. 2023, 62, 11278–11286

(Table 1) and photoluminescence maxima well beyond 650 nm (Figure 5 and Table 2). Importantly, the high $\Phi_{PL}$ values observed in the red region are maintained for these lower-energy emitters. In **CNpiq-L$^1$**, which luminesces with a maximum near 700 nm, $\Phi_{PL}$ = 0.48 in solution, augmenting to 0.65 in PMMA. In **CNpiq-L$^5$**, which is not as deep red, exceptional $\Phi_{PL}$ values of 0.76 (toluene solution) and 0.84 (PMMA film) are observed. These compounds represent some of the most efficient deep-red phosphors known and show that the salicylaldimine and 2-picolinamide ligand classes developed here are particularly effective in this region of the spectrum.

## CONCLUSIONS

To summarize, we developed two ancillary ligand classes that support efficient bis-cyclometalated iridium red phosphors. These electron-rich ancillary ligands enable a large radiative rate constant, $k_r$. Ligand substituents play a large role in controlling the nonradiative rate constant ($k_{nr}$) in a fluid solution, which allows the photoluminescence quantum yield, $\Phi_{PL}$, to be optimized. Some notable advantages of these classes of ancillary ligands emerge when comparing to other types of electron-rich L^X ligands that have been previously used in red-phosphorescent compounds. First, the synthetic chemistry is simplified, using air and moisture-stable precursors, and generating products that are robust under ambient conditions and amenable to chromatographic purification. Moreover, the chemically distinct and unconjugated "L" and "X" functionalities can be modified separately, and we showed here that substituent effects on both parts can play major roles in optimizing the photoluminescence. Finally, the large impacts on excited-state dynamics occur with minimal changes in the $T_1$ energy and the accompanying phosphorescence spectrum, allowing the phosphorescence efficiency to be optimized without alteration of the emission color profile. Another important insight from this work is that the optimum salicylaldimine ligand (**L$^1$**) and 2-picolinamide ligand (**L$^5$**), selected from a survey of five red-emitting C^N = piq complexes, also perform exemplarily in cyano-substituted compounds that luminesce deeper in the red and near-infrared region. This work produced several red phosphors with exceptional photoluminescence quantum yields and motivates future studies and applications of compounds supported by these classes of ancillary ligands.

## ASSOCIATED CONTENT

### Supporting Information

The Supporting Information is available free of charge at https://pubs.acs.org/doi/10.1021/acs.inorgchem.3c01770.

X-ray crystallography summary table, NMR spectra, mass spectrometry data, excitation spectra, low-temperature emission spectra, and time-resolved photoluminescence data (PDF)

### Accession Codes

CCDC 2242186−2242190 contain the supplementary crystallographic data for this paper. The data can be obtained free of charge via www.ccdc.cam.ac.uk/data_request/cif, or by emailing data_request@ccdc.cam.ac.uk, or by contacting The Cambridge Crystallographic Data Centre, 12 Union Road, Cambridge CB2 1EZ, UK; fax: + 44 1223 336033.

## AUTHOR INFORMATION


### Corresponding Author

**Thomas S. Teets** − *University of Houston, Department of Chemistry, Houston, Texas 77204-5003, United States;* orcid.org/0000-0002-7471-8467; Email: tteets@uh.edu

### Authors

**Chenggang Jiang** − *University of Houston, Department of Chemistry, Houston, Texas 77204-5003, United States;* orcid.org/0000-0002-2240-831X

**Sungwon Yoon** − *University of Houston, Department of Chemistry, Houston, Texas 77204-5003, United States*

**Yennie H. Nguyen** − *University of Houston, Department of Chemistry, Houston, Texas 77204-5003, United States;* orcid.org/0000-0002-4474-6176

Complete contact information is available at: https://pubs.acs.org/10.1021/acs.inorgchem.3c01770


### Author Contributions

The manuscript was written through contributions of all authors. All authors have given approval to the final version of the manuscript.

### Notes

The authors declare no competing financial interest.

## ACKNOWLEDGMENTS

We acknowledge the National Science Foundation (Grant CHE-1846831) and the Welch Foundation (Grant E-1887) for funding this work.

## REFERENCES


(1) Zhang, M.; Qian, M.; Huang, H.; Gao, Q.; Zhang, C.; Qi, H. Carboxyl Group Bearing Iridium(III) Solvent Complex as Photoluminescence and Electrochemiluminescence Probe for the Detection of Histidine. *J. Electroanal. Chem.* **2022**, *920*, No. 116578.

(2) Feng, Z.; Xian, J.; Chen, F.; Wang, Y.; Tian, Y.; Sun, J.; Tian, X. Intermolecular Interactions Enhanced Second Harmony Generation of Iridium Complex for Bio-Labeling. *Chem. Eng. J.* **2023**, *458*, No. 141503.

(3) DiSalle, B. F.; Bernhard, S. Orchestrated Photocatalytic Water Reduction Using Surface-Adsorbing Iridium Photosensitizers. *J. Am. Chem. Soc.* **2011**, *133* (31), 11819−11821.

(4) Xu, L.; Deng, P.; Song, W.; Liu, M.; Wang, M.; Yu, Y.; Wang, F. An AIE-Active Cyclometalated Iridium(III) Photosensitizer for Selective Discrimination, Imaging, and Synergistic Elimination of Gram-Positive Bacteria. *ACS Mater. Lett.* **2023**, *5* (1), 162−171.

(5) Cho, J.-Y.; Tse, M. K.; Holmes, D.; Maleczka, R. E.; Smith, M. R. Remarkably Selective Iridium Catalysts for the Elaboration of Aromatic C-H Bonds. *Science* **2002**, *295* (5553), 305−308.

(6) Li, H.; Fei, M.; Troiano, J. L.; Ma, L.; Yan, X.; Tieu, P.; Yuan, Y.; Zhang, Y.; Liu, T.; Pan, X.; Brudvig, G. W.; Wang, D. Selective Methane Oxidation by Heterogenized Iridium Catalysts. *J. Am. Chem. Soc.* **2023**, *145* (2), 769−773.

(7) Wu, Y.; Sutton, G. D.; Halamicek, M. D. S.; Xing, X.; Bao, J.; Teets, T. S. Cyclometalated Iridium-Coumarin Ratiometric Oxygen Sensors: Improved Signal Resolution and Tunable Dynamic Ranges. *Chem. Sci.* **2022**, *13* (30), 8804−8812.

(8) Yoshihara, T.; Matsumura, N.; Tamura, T.; Shiozaki, S.; Tobita, S. Intracellular and Intravascular Oxygen Sensing of Pancreatic Tissues Based on Phosphorescence Lifetime Imaging Microscopy Using Lipophilic and Hydrophilic Iridium(III) Complexes. *ACS Sens.* **2022**, *7* (2), 545−554.

(9) Idris, M.; Kapper, S. C.; Tadle, A. C.; Batagoda, T.; Muthiah Ravinson, D. S.; Abimbola, O.; Djurovich, P. I.; Kim, J.; Coburn, C.; Forrest, S. R.; Thompson, M. E. Blue Emissive Fac/Mer-Iridium (III)

NHC Carbene Complexes and Their Application in OLEDs. *Adv. Opt. Mater.* **2021**, *9* (8), No. 2001994.
(10) Hong, G.; Gan, X.; Leonhardt, C.; Zhang, Z.; Seibert, J.; Busch, J. M.; Bräse, S. A Brief History of OLEDs—Emitter Development and Industry Milestones. *Adv. Mater.* **2021**, *33* (9), No. 2005630.
(11) Penconi, M.; Kajjam, A. B.; Jung, M.-C.; Cazzaniga, M.; Baldoli, C.; Ceresoli, D.; Thompson, M. E.; Bossi, A. Advancing Near-Infrared Phosphorescence with Heteroleptic Iridium Complexes Bearing a Single Emitting Ligand: Properties and Organic Light-Emitting Diode Applications. *Chem. Mater.* **2022**, *34* (2), 574−583.
(12) Liang, X.; Zhang, F.; Yan, Z.-P.; Wu, Z.-G.; Zheng, Y.; Cheng, G.; Wang, Y.; Zuo, J.-L.; Pan, Y.; Che, C.-M. Fast Synthesis of Iridium(III) Complexes Incorporating a Bis(Diphenylphorothioyl)-Amide Ligand for Efficient Pure Green OLEDs. *ACS Appl. Mater. Interfaces* **2019**, *11* (7), 7184−7191.
(13) Baldo, M. A.; O'Brien, D. F.; You, Y.; Shoustikov, A.; Sibley, S.; Thompson, M. E.; Forrest, S. R. Highly Efficient Phosphorescent Emission from Organic Electroluminescent Devices. *Nature* **1998**, *395* (6698), 151−154.
(14) Smith, A. R. G.; Burn, P. L.; Powell, B. J. Spin−Orbit Coupling in Phosphorescent Iridium(III) Complexes. *ChemPhysChem* **2011**, *12* (13), 2429−2438.
(15) Nazeeruddin, Md. K.; Humphry-Baker, R.; Berner, D.; Rivier, S.; Zuppiroli, L.; Graetzel, M. Highly Phosphorescence Iridium Complexes and Their Application in Organic Light-Emitting Devices. *J. Am. Chem. Soc.* **2003**, *125* (29), 8790−8797.
(16) Sajoto, T.; Djurovich, P. I.; Tamayo, A. B.; Oxgaard, J.; Goddard, W. A. I.; Thompson, M. E. Temperature Dependence of Blue Phosphorescent Cyclometalated Ir(III) Complexes. *J. Am. Chem. Soc.* **2009**, *131* (28), 9813−9822.
(17) Tao, P.; Li, W.-L.; Zhang, J.; Guo, S.; Zhao, Q.; Wang, H.; Wei, B.; Liu, S.-J.; Zhou, X.-H.; Yu, Q.; Xu, B.-S.; Huang, W. Facile Synthesis of Highly Efficient Lepidine-Based Phosphorescent Iridium-(III) Complexes for Yellow and White Organic Light-Emitting Diodes. *Adv. Funct. Mater.* **2016**, *26* (6), 881−894.
(18) Li, T.-Y.; Wu, J.; Wu, Z.-G.; Zheng, Y.-X.; Zuo, J.-L.; Pan, Y. Rational Design of Phosphorescent Iridium(III) Complexes for Emission Color Tunability and Their Applications in OLEDs. *Coord. Chem. Rev.* **2018**, *374*, 55−92.
(19) Tsuboyama, A.; Iwawaki, H.; Furugori, M.; Mukaide, T.; Kamatani, J.; Igawa, S.; Moriyama, T.; Miura, S.; Takiguchi, T.; Okada, S.; Hoshino, M.; Ueno, K. Homoleptic Cyclometalated Iridium Complexes with Highly Efficient Red Phosphorescence and Application to Organic Light-Emitting Diode. *J. Am. Chem. Soc.* **2003**, *125* (42), 12971−12979.
(20) Deaton, J. C.; Young, R. H.; Lenhard, J. R.; Rajeswaran, M.; Huo, S. Photophysical Properties of the Series *Fac-* and *Mer-*(1-Phenylisoquinolinato-N^C$^{2'}$)$_x$(2-Phenylpyridinato-N^C$^{2'}$)$_{3-x}$Iridium-(III)($x$ = 1−3). *Inorg. Chem.* **2010**, *49* (20), 9151−9161.
(21) Fleetham, T.; Li, G.; Li, J. Efficient Red-Emitting Platinum Complex with Long Operational Stability. *ACS Appl. Mater. Interfaces* **2015**, *7* (30), 16240−16246.
(22) Tuong Ly, K.; Chen-Cheng, R.-W.; Lin, H.-W.; Shiau, Y.-J.; Liu, S.-H.; Chou, P.-T.; Tsao, C.-S.; Huang, Y.-C.; Chi, Y. Near-Infrared Organic Light-Emitting Diodes with Very High External Quantum Efficiency and Radiance. *Nat. Photonics* **2017**, *11* (1), 63−68.
(23) Carlson, B.; Phelan, G. D.; Kaminsky, W.; Dalton, L.; Jiang, X.; Liu, S.; Jen, A. K.-Y. Divalent Osmium Complexes: Synthesis, Characterization, Strong Red Phosphorescence, and Electrophosphorescence. *J. Am. Chem. Soc.* **2002**, *124* (47), 14162−14172.
(24) Englman, R.; Jortner, J. The Energy Gap Law for Radiationless Transitions in Large Molecules. *Mol. Phys.* **1970**, *18* (2), 145−164.
(25) Yersin, H. *Highly Efficient OLEDs with Phosphorescent Materials*; John Wiley & Sons, 2008.
(26) Qian, G.; Wang, Z. Y. Near-Infrared Organic Compounds and Emerging Applications. *Chem. − Asian J.* **2010**, *5* (5), 1006−1029.
(27) Wu, W.; Zhang, C.; Rees, T. W.; Liao, X.; Yan, X.; Chen, Y.; Ji, L.; Chao, H. Lysosome-Targeting Iridium(III) Probe with Near-Infrared Emission for the Visualization of NO/$O_2^{\bullet-}$ Crosstalk via In Vivo Peroxynitrite Imaging. *Anal. Chem.* **2020**, *92* (8), 6003−6009.
(28) Wu, W.; Liao, X.; Chen, Y.; Ji, L.; Chao, H. Mitochondria-Targeting and Reversible Near-Infrared Emissive Iridium(III) Probe for in Vivo ONOO−/GSH Redox Cycles Monitoring. *Anal. Chem.* **2021**, *93* (22), 8062−8070.
(29) Lamansky, S.; Djurovich, P.; Murphy, D.; Abdel-Razzaq, F.; Lee, H.-E.; Adachi, C.; Burrows, P. E.; Forrest, S. R.; Thompson, M. E. Highly Phosphorescent Bis-Cyclometalated Iridium Complexes: Synthesis, Photophysical Characterization, and Use in Organic Light Emitting Diodes. *J. Am. Chem. Soc.* **2001**, *123* (18), 4304−4312.
(30) Li, J.; Djurovich, P. I.; Alleyne, B. D.; Yousufuddin, M.; Ho, N. N.; Thomas, J. C.; Peters, J. C.; Bau, R.; Thompson, M. E. Synthetic Control of Excited-State Properties in Cyclometalated Ir(III) Complexes Using Ancillary Ligands. *Inorg. Chem.* **2005**, *44* (6), 1713−1727.
(31) Lai, P.-N.; Brysacz, C. H.; Alam, M. K.; Ayoub, N. A.; Gray, T. G.; Bao, J.; Teets, T. S. Highly Efficient Red-Emitting Bis-Cyclometalated Iridium Complexes. *J. Am. Chem. Soc.* **2018**, *140* (32), 10198−10207.
(32) Lai, P.; Yoon, S.; Wu, Y.; Teets, T. S. Effects of Ancillary Ligands on Deep Red to Near-Infrared Cyclometalated Iridium Complexes. *ACS Org. Inorg. Au* **2022**, *2* (3), 236−244.
(33) Kabir, E.; Wu, Y.; Sittel, S.; Nguyen, B.-L.; Teets, T. S. Improved Deep-Red Phosphorescence in Cyclometalated Iridium Complexes via Ancillary Ligand Modification. *Inorg. Chem. Front.* **2020**, *7* (6), 1362−1373.
(34) Yoon, S.; Teets, T. S. Enhanced Deep Red to Near-Infrared (DR-NIR) Phosphorescence in Cyclometalated Iridium(III) Complexes. *Inorg. Chem. Front.* **2022**, *9* (24), 6544−6553.
(35) Lu, G.-Z.; Zhu, Q.; Liu, L.; Wu, Z.-G.; Zheng, Y.-X.; Zhou, L.; Zuo, J.-L.; Zhang, H. Pure Red Iridium(III) Complexes Possessing Good Electron Mobility with 1,5-Naphthyridin-4-Ol Derivatives for High-Performance OLEDs with an EQE over 31%. *ACS Appl. Mater. Interfaces* **2019**, *11* (22), 20192−20199.
(36) Kim, H. U.; Jang, H. J.; Choi, W.; Kim, M.; Park, S.; Park, T.; Lee, J. Y.; K. S., B. Ancillary Ligand-Assisted Robust Deep-Red Emission in Iridium(III) Complexes for Solution-Processable Phosphorescent OLEDs. *J. Mater. Chem. C* **2019**, *7* (14), 4143−4154.
(37) Yoon, S.; Teets, T. S. Red to Near-Infrared Phosphorescent Ir(III) Complexes with Electron-Rich Chelating Ligands. *Chem. Commun.* **2021**, *57* (16), 1975−1988.
(38) Zhao, Q.; Li, L.; Li, F.; Yu, M.; Liu, Z.; Yi, T.; Huang, C. Aggregation-Induced Phosphorescent Emission (AIPE) of Iridium-(III) Complexes. *Chem. Commun.* **2008**, No. 6, 685−687.
(39) You, Y.; Huh, H. S.; Kim, K. S.; Lee, S. W.; Kim, D.; Park, S. Y. Comment on 'Aggregation-Induced Phosphorescent Emission (AIPE) of Iridium(III) Complexes': Origin of the Enhanced Phosphorescence. *Chem. Commun.* **2008**, No. 34, 3998−4000.
(40) Howarth, A. J.; Patia, R.; Davies, D. L.; Lelj, F.; Wolf, M. O.; Singh, K. Elucidating the Origin of Enhanced Phosphorescence Emission in the Solid State (EPESS) in Cyclometallated Iridium Complexes. *Eur. J. Inorg. Chem.* **2014**, *2014* (23), 3657−3664.
(41) Li, T.-Y.; Zheng, Y.-X.; Zhou, Y.-H. Iridium(III) Phosphorescent Complexes with Dual Stereogenic Centers: Single Crystal, Electronic Circular Dichroism Evidence and Circularly Polarized Luminescence Properties. *Dalton Trans.* **2016**, *45* (48), 19234−19237.
(42) Pal, S.; Joy, S.; Paul, H.; Banerjee, S.; Maji, A.; Zangrando, E.; Chattopadhyay, P. Understanding the Difference in Photophysical Properties of Cyclometalated Iridium(III) and Rhodium(III) Complexes by Detailed Time-Dependent Density Functional Theory and Frontier Molecular Orbital Supports. *J. Phys. Chem. C* **2017**, *121* (21), 11632−11642.
(43) Chandrasekhar, V.; Mahanti, B.; Pandey, M. D.; Narayanan, R. S. Cyclometalated Ir(III) Complex as a Metalloligand and a Selective Cu(II) Sensor: Synthesis and Structural Characterization of a Heterometallic Tetranuclear Ir(III)/Cu(II) Complex. *ACS Omega* **2018**, *3* (3), 2786−2792.


https://doi.org/10.1021/acs.inorgchem.3c01770
*Inorg. Chem.* 2023, 62, 11278−11286

(44) Chandrasekhar, V.; Mahanti, B.; Bandipalli, P.; Bhanuprakash, K.; Nair, N. N. Cyclometalated Ir(III) Complexes Containing N-Aryl Picolinamide Ancillary Ligands. *J. Organomet. Chem.* **2011**, *696* (14), 2711−2719.
(45) You, Y.; Park, S. Y. Inter-Ligand Energy Transfer and Related Emission Change in the Cyclometalated Heteroleptic Iridium Complex: Facile and Efficient Color Tuning over the Whole Visible Range by the Ancillary Ligand Structure. *J. Am. Chem. Soc.* **2005**, *127* (36), 12438−12439.
(46) Lai, P.; Teets, T. S. Ancillary Ligand Effects on Red-Emitting Cyclometalated Iridium Complexes. *Chem. − Eur. J.* **2019**, *25* (23), 6026−6037.
(47) Nonoyama, M. Benzo[h]Quinolin-10-Yl-N Iridium(III) Complexes. *Bull. Chem. Soc. Jpn.* **1974**, *47* (3), 767−768.
(48) Kovaříček, P.; Lehn, J.-M. Merging Constitutional and Motional Covalent Dynamics in Reversible Imine Formation and Exchange Processes. *J. Am. Chem. Soc.* **2012**, *134* (22), 9446−9455.
(49) Yin, X.-F.; Lin, H.; Jia, A.-Q.; Chen, Q.; Zhang, Q.-F. Synthesis, Structural Characterization, and Catalytic Activity of Ruthenium(II) Monocarbonyl Complexes with Bidentate Schiff Base and Triphenylphosphine Ligands. *J. Coord. Chem.* **2013**, *66* (18), 3229−3240.
(50) Cheng, T.-J.; Wang, X.; Xu, H.; Dai, H.-X. Copper-Mediated Ortho CH Primary Amination of Anilines. *Tetrahedron Lett.* **2021**, *73*, No. 153099.
(51) Bian, Y.-J.; Chen, C.-Y.; Huang, Z.-Z. Synthesis of Imides by Palladium-Catalyzed C−H Functionalization of Aldehydes with Secondary Amides. *Chem. − Eur. J.* **2013**, *19* (3), 1129−1133.
(52) Sheldrick, G. M. Crystal Structure Refinement with SHELXL. *Acta Crystallogr. Sect. C Struct. Chem.* **2015**, *71* (1), 3−8.
(53) Spek, A. L. Structure Validation in Chemical Crystallography. *Acta Crystallogr. D Biol. Crystallogr.* **2009**, *65* (2), 148−155.
(54) Espinoza, E. M.; Clark, J. A.; Soliman, J.; Derr, J. B.; Morales, M.; Vullev, V. I. Practical Aspects of Cyclic Voltammetry: How to Estimate Reduction Potentials When Irreversibility Prevails. *J. Electrochem. Soc.* **2019**, *166* (5), H3175−H3187.
(55) Fan, C.-H.; Sun, P.; Su, T.-H.; Cheng, C.-H. Host and Dopant Materials for Idealized Deep-Red Organic Electrophosphorescence Devices. *Adv. Mater.* **2011**, *23* (26), 2981−2985.


https://doi.org/10.1021/acs.inorgchem.3c01770
*Inorg. Chem.* 2023, 62, 11278−11286